Proceedings World Geothermal Congress 2015
Melbourne, Australia, 19-25 April 2015

Dual Porosity Models of a Two-phase Geothermal Reservoir

Jaime Jemuel C. Austria, Jr.[1, 2], Michael J. O'Sullivan[2]

[1]Energy Development Corporation, 38/F One Corporate Centre Building, Julia Vargas, Pasig 1605, Philippines

[2]Department of Engineering Science, University of Auckland, Auckland 1010 New Zealand

austria.jjc@energy.com.ph; m.osullivan@auckland.ac.nz

Keywords: Geothermal, reservoir simulation, dual porosity, MINC, Mt. Apo geothermal production field

ABSTRACT

The research reported here is part of a general study aimed at determining when dual porosity models should be preferred ahead of single porosity models for modeling geothermal systems. The Mt. Apo geothermal reservoir, in Mindanao, Philippines, was simulated using both single and dual porosity models and inverse modeling was used to estimate permeabilities and porosities. The Mt. Apo system was selected as a test case because it consists of low to moderate permeability fractured rock and some of the wells produce high enthalpy fluid. Both of these factors make it likely that a dual porosity model may be useful.

The forward simulations were carried out with AUTOUGH2 (Yeh *et al.*, 2012), a modified version of TOUGH2 (Pruess, 1991) while the inverse problem of determining the best-fit parameters for the dual natural-state and production history model calibration was solved using PEST (Doherty, 2010). The model was calibrated using steady-state temperatures and pressure data, and monthly average monthly enthalpy data for a period of 16.2 years.

The results were compared for a single porosity model and various dual porosity models with the aim of determining whether or not one type of model clearly fitted the data better than the others. A dual porosity model gives the best match to the measured production enthalpies.

1. INTRODUCTION

The main objective of this work is to determine how the results from single and dual porosity models compare for simulations of the production history of a two-phase geothermal reservoir such as the Mt. Apo geothermal reservoir in the Philippines. The fractured nature of the reservoir, the presence of a steam zone in the natural-state, the occurrence of wells that intersect the steam zone and discharge high enthalpy fluid makes the Mt Apo geothermal reservoir a good test case for modeling with the dual porosity approach.

The Mt. Apo geothermal field is located inside the 7.01-km^2 Mt. Apo geothermal reservation area in the south-eastern part of the island of Mindanao in the Philippines (See Figure 1.) Mt. Apo at 2,954 masl is the highest peak in the Philippines. The main features of the Mt. Apo geothermal reservoir are the Sandawa Collapse, the Marbel Corridor, and the Matingao segment. The Mt. Apo geothermal reservoir is characterized by very high reservoir temperatures (>300°C) and neutral chloride production fluid (Trazona *et al.*, 2002). The main reservoir of the Mt. Apo geothermal system is controlled by fractures, with the upwelling fluid flowing horizontally to the northwest through the northwest-southeast trending faults in the Marbel Corridor which serve as paths for fluid flow (Esberto and Sarmiento, 1999). To the west of Marbel is the Matingao sector which is characterized by lower temperature fluids (<220°C). Recharge comes from nearby areas of higher elevation, driven by the topography. Meteoric water derived from abundant rainfall and descending cold water provide deep recharge to the reservoir (Esberto *et al.*, 1998).

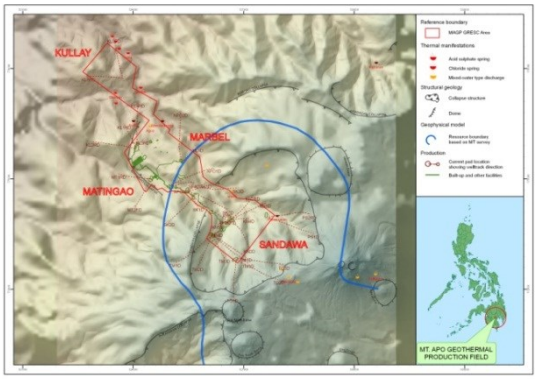

Figure 1: Location of Mt. Apo geothermal field, modified after Emoricha *et al.* (2002)

In the natural state the vertical distribution of pressure in the Mt. Apo geothermal reservoir is approximately liquid-hydrostatic (~8.2 kPa/m). When the wells with liquid-hydrostatic pressure profile were first discharged, the production enthalpy of some of them was very high, with some of the wells discharging almost dry steam. This phenomenon was attributed to the presence of a shallow steam zone beneath the Sandawa Collapse and extending above the outflow toward the Marbel Corridor in the undisturbed

reservoir (Esberto and Sarmiento, 1999). This natural state steam zone underneath the Sandawa collapse appears to be formed by continuous boiling in the upflow portion of the reservoir at about -250 mrsl (Esberto, 1995).

During the early stages of production, the average field enthalpy increased because of pressure drawdown and the high enthalpy fluid coming from two phase steam dominated wells SK2D, SK3D, SK4D, SK5D, and SK6D. These wells discharged two-phase fluid with increasing production enthalpy ranging between 1200 kJ/kg and 1500 kJ/kg (Esberto and Sarmiento, 1999). Well SK1D which intersected the permeable northwest trending structures and the outer rim of the Sandawa collapse in the Marbel sector initially produced steam-dominated fluid with an enthalpy of 2030 kJ/kg (Trazona *et al.*, 2002) which then increased to 2700 kJ/kg. In order to improve the connectivity to the reservoir and gain a higher contribution from the steam zones, the production casing of well SK1D was perforated and the perforated zones were acidized (Buning *et al.*, 1997; Molina *et al.*, 1998). The wells KN2D, KN3B and KN5D in Kanlas and TM1D, TM2D, TM3D and TM4D in the Tambaan sector (Esberto and Sarmiento, 1999; Trazona *et al.*, 2002) also tapped the natural state steam zone and discharged steam-dominated fluid with production enthalpies ranging between 1500 kJ/kg and 2700 kJ/kg.

The high enthalpy two-phase steam-dominated discharge of wells such as SK1D, KN2D, KN3D, KN5D, TM3D, and TM4D is thought to be associated with two-phase flow of a water/steam mixture in high permeability fractures of limited volume within a tight matrix (Pritchett, 2005). The high energy content of the low permeability matrix blocks makes the fluid in the matrix blocks boil as it enters the fractures. Heat conduction in the matrix blocks also helps to maintain the boiling in the fractures.

According to Pritchett (2005), the high-enthalpy and steam-dominated discharge of geothermal wells is related to high local heterogeneity in the reservoir with a sharp permeability contrast between a relatively impermeable rock matrix and the high permeability fracture zones, and he further concluded that dual porosity models are required for simulating this type of behavior. Examples of the use of dual porosity models to simulate the excess enthalpies of production wells in high-enthalpy and steam-dominated reservoirs during exploitation include the modeling studies of The Geysers geothermal field in USA (Bodvarsson and Witherspoon, 1985), Krafla geothermal field in Iceland (Finsterle *et al.*, 1999), Los Azufres geothermal field in Mexico (Jaimes-Maldonado *et al.*, 2005), Uenotai geothermal field in northern Honshu, Japan (Nakao *et al.*, 2007), and the Mutnovsky geothermal field in Russia (Kiryukhin and Miroshnik, 2012).

2. EARLY MODELS OF THE MT. APO GEOTHERMAL RESERVOIR

2.1 The early conceptual models

The early conceptual model of Mt. Apo (Esberto, 1995; Esberto and Sarmiento, 1999) postulated a main upflow beneath the Sandawa collapse in the south-eastern part of the reservoir. A two-phase zone overlies the single-phase fluid in the reservoir from 0 mrsl to -250 mrsl. The discharge fluid from well KN3B, which was drilled down to 1600 m below sea level beneath the Sandawa collapse, was found to characterize the main upflow fluid. The discharge fluid from this well has a temperature of >300°C, 6000 ppm Cl content, and 80 mmols/100 mols of CO_2 content (Trazona *et al.*, 2002). The entire northwest-trending magnetotelluric (MT) anomaly delineated by the >50-Ω-m shallow resistive basement at sea level defines most likely extent of the high temperature region of the Mindanao hydrothermal system (Los Baños *et al.*, 2010).

The main upflow moves horizontally to the northwest and is channeled by various northwest-southeast trending faults in the Marbel Corridor which serve as paths for fluid flow. The outflow is characterised by a reversal in the temperature with depth profiles of the wells drilled in the Kullay and Matingao sectors. The outflow is diverted to the north by an impermeable sector in Matingao and moved towards well APO2D. The <30Ω-m conductive zones delineates the outer resource boundary while the widespread low resistivity to the northwest demarcates the major outflow towards Agco, Imba and Marbel thermal springs. The outflow finally come up to surface as chloride springs in Imba, Marbel and Sisiman through the quatenary volcanics and quatenary pyroclastics (Los Baños *et al.*, 2010).

2.2 The volumetric model

The Mt. Apo geothermal reserve capacity was first estimated using a probabilistic (Monte Carlo) volumetric stored heat calculation. The reserve capacity was estimated to be at least 292 MWe for 25 years (Sarmiento and Björnsson, 2007; Sussman *et al.*, 1993). When more production data became available, these early estimates of geothermal reserves were validated by distributed parameter models presented by Esberto and Sarmiento (1999) and Emoricha *et al.* (2010).

2.3 The numerical model of Esberto (1995)

The first three dimensional numerical model of the Mt. Apo geothermal reservoir was developed by Esberto (1995) using the computer code MULKOM (Pruess, 1983). It was a single porosity model and it was created in order to evaluate the response of the reservoir to a generating capacity of 52 MWe. The model had its surface set at the water table and was based on a rectangular grid consisting of 88 computational elements. The model grid covered an area of 130 km^2 and extended to -2000 mrsl, with nine layers of variable thickness. The grid was oriented in the northwest-southeast direction, parallel to the Marbel fault zone.

The numerical model presented by Esberto (1995) was calibrated against natural state downhole temperature and pressure data. The best-fit natural-state model was able to reasonably match the main reservoir characteristics as described in the conceptual model. The natural-state model was used as the initial condition for a production history model. The production history model was calibrated against the measured enthalpy from eight production wells (APO1D, APO3D, SP4D, SK2D, SK4B, SK5D, SK6D and SK3D). The simulation results from the production history model showed good matches to the enthalpy from wells with a low enthalpy discharge. However, the vapor saturation steam zone that evolved during the natural state was not dry enough (Esberto, 1995) and as a result the model underestimated the production enthalpy for the steam-dominated wells.

2.4 The numerical model of Esberto and Sarmiento (1999)

The model presented by Esberto (1995) was updated by Esberto and Sarmiento (1999) and was used for investigating the response of the reservoir to an increased generating capacity of 102 MWe. The three dimensional single porosity model was developed using the TETRAD reservoir simulator (Vinsome and Shook, 1993). The model had a rectangular grid with a total of 1,122 computational elements. The model grid covered a smaller area of only 60 km^2, extended to a shallower depth of -1500 mrsl, and had fewer layers (only 6) compared to the grid used by Esberto (1995). The resistivity boundary area, the Marbel corridor, and the Matingao block are inside the model boundary. The grid was also rotated and aligned along a direction parallel to the Marbel fault zone. The model was assigned rock permeabilities based on the injectivities and production capacity of the wells while background permeability was assumed for blocks for which there was no well test data.

The numerical model presented by Esberto and Sarmiento (1999) was matched against natural-state downhole temperature and pressure data from production and injection wells. The production history model was calibrated against production enthalpy data from the nine production wells which were supplying high-pressure steam to the 52-MWe power station. The match of the simulation results to downhole temperature and pressure data was reasonably good. The match of the production history model to the enthalpy data from the production wells with a medium to low discharge enthalpy was also reasonably good. However, the match of simulated enthalpies with the enthalpy data from the two-phase steam-dominated wells was not good, again because the vapor saturation obtained was not high enough.

2.5 The numerical model of Emoricha *et al.* (2010)

Emoricha *et al.* (2010) carried out an update of the numerical model of Esberto and Sarmiento (1999) in order to investigate the feasibility of producing 154 MWe, thus increasing the capacity by 50MWe. The three dimensional single porosity model was developed using TOUGH2 (Pruess, 1991). The model had its top set at the water table and the elevation at the top of each column of the model was fitted to the water table data. The model grid covered a much larger area (572 km^2) and extended deeper (-2000 mrsl) compared to the models of Esberto (1995) or Esberto and Sarmiento (1999). There were 19 layers in the model with each layer consisting of 1,457 elements thus giving a total of 27,683 computational elements. The 7.01 km^2 Mt. Apo geothermal reservation is at the centre of the model grid.

The grid also covered the entire northwest-trending magnetotelluric (MT) anomaly defined by the >50-Ω-m shallow resistive basement at sea level and thus covered the most likely extent of the high temperature region of the Mindanao hydrothermal system (Los Baños *et al.*, 2010). The model grid was oriented in the northwest-southeast direction, generally parallel to the Marbel fault zone and consistent with the interpretation of the MT data which indicated a northwest trending MT anomaly characterizing the shallow electrical basement between the western flanks of Mt. Apo and eastern slopes of Mt. Zion (Los Baños *et al.*, 2010). The permeability distribution was generally based on the Mt. Apo reservoir simulation study of Esberto and Sarmiento (1999).

The production history model was calibrated against the enthalpy data from 19 production wells. The production history model was able to reproduce the observed effects of injected fluids and the expansion of the two-phase zones. The simulated enthalpy was lower than the enthalpy data for the two-phase liquid-dominated wells. For the two-phase steam-dominated wells, the simulated enthalpy fluctuated and thus was not able to provide a consistent match to the enthalpy data. Nevertheless, the enthalpy matches were deemed to be acceptable and the numerical model was used for predictive purposes. The predictive model showed that another 50MWe of generating capacity was viable and would not result to a significant pressure drawdown in the reservoir. The model presented by Emoricha *et al.* (2010) was updated by the Energy Development Corporation (EDC) in collaboration with the University of Auckland in 2011, both to improve the model and to review the reservoir modeling processes used by EDC.

3. DUAL POROSITY MODELLING STUDY

The previous studies all used single porosity models but in the present study the Mt. Apo geothermal reservoir is modeled using both the single and dual porosity approach. The aim is to determine which type of model fits the observed data best and therefore which type of model should be preferred for modeling high enthalpy, two-phase geothermal systems.

3.1 Modeling approach

3.1.1 Single porosity model

The single porosity approach is an idealization of flow in fractured media where the physical quantities in the fracture and the adjacent rock matrix, such as permeability, porosity, pressure and temperature, are averaged over large blocks of materials containing a large number of fractures (Narasimhan, 1982).

Single porosity models have often been used for modeling geothermal reservoirs. A few examples include:

(i) Two-phase, low-enthalpy geothermal reservoirs such as Momotombo in Nicaragua (Porras *et al.*, 2007), and Wairakei in New Zealand (O'Sullivan *et al.*, 2009).

(ii) Two-phase, medium-enthalpy geothermal reservoirs such as Berlin in El Salvador (Monterrosa, 2002), and Nesjavellir in Iceland (Bjornsson *et al.*, 2003; Steingrimsson *et al.*, 2000).

(iii) Two-phase, high-enthalpy geothermal reservoirs such as Olkaria (Bodvarsson *et al.*, 1987; Ofwona, 2002), Bacon-Manito in the Philippines (Austria, 2008), and Mt. Apo in the Philippines (Emoricha *et al.*, 2010; Esberto and Sarmiento, 1999).

(iv) Two-phase, steam-dominated geothermal reservoirs such as Lahendong in North Sulawesi in Indonesia (Yani, 2006), and Kamojang in Indonesia (Suryadarma *et al.*, 2010).

3.1.2 Dual porosity model

The dual porosity approach idealizes the flow region as two interacting continua, namely the fractures and the matrix. The concept was introduced by Barenblatt *et al.* (1960) for representing the seepage of homogenous fluids in fissured rocks. In the dual porosity approach for representing a fracture network in a low permeability rock matrix, it is assumed that the fluid flows mainly through the fractures and hence the matrix to matrix flow is negligible (Warren and Root, 1963; Zimmerman *et al.*, 1996). The multiple interacting continua or MINC method in TOUGH2 adds further complexity to the dual porosity approach by allowing the matrix to be subdivided into nested blocks (Pruess and Narasimhan, 1985), thus representing gradients of pressure, temperature or concentration inside the matrix. Some examples of two-phase and steam-dominated geothermal reservoirs that have been modeled using the dual porosity approach are:

(i) Two-phase, low-enthalpy geothermal reservoirs such as Mori in Japan (Osada *et al.*, 2010), Oguni in Japan (Nakanishi *et al.*, 1995), and Ribeira Grande, São Miguel, Azores in Portugal (Pham *et al.*, 2010).

(ii) Two-phase, medium-enthalpy geothermal reservoirs such Cerro Prieto in Mexico (Butler *et al.*, 2000), Ngatamariki in New Zealand (Clearwater *et al.*, 2012).

(iii) Two-phase, high-enthalpy geothermal reservoirs such Los Azufres in Mexico (Jaimes-Maldonado *et al.*, 2005), Rotokawa in New Zealand (Bowyer and Holt, 2010), and Mutnovsky in Kamchatka, Russia (Kiryukhin and Miroshnik, 2012).

(v) Two-phase, steam-dominated geothermal reservoirs such as Geysers in the USA (Williamson, 1990).

3.2 Model description

3.2.1 Single porosity model

The single porosity model of Mt. Apo used here is generally based on the model presented by Emoricha *et al.* (2010) but has a more refined model grid with 106% more grid blocks. It was first developed in TOUGH2 and then converted into a form recognisable by AUTOUGH (Yeh *et al.*, 2012). As with the previous models, the model grid was rotated by 45° to align the model northwest-southeast parallel to the Marbel fault zone. The model has an area of 600 km^2 and covers the resource boundary delineated by the MT results of Los Baños *et al.* (2010). The grid was chosen to be large enough so that the model is infinite acting with no changes in the outer blocks observed in any of the simulations.

The updated model for Mt. Apo has 17 layers and a single atmospheric block on top. The layers have varying thicknesses as follows: 600m (bottom layer 1), 400m (layer 2), 300m (layers 3 and 4), and 200m (layers 5 to 16). Layers 13 to 17 have variable thicknesses since the top of the model follows the water table. The model has a depth ranging from 3.4 km at the edges to 4.2 km at the centre. The model has 3,555 elements per layer from layers 1 to 13. The number of element then varies from layer 14 to 17 because the model follows the water table contour. The model has a total of 57,125 elements (see Figure 2) which is twice the number of elements used in the model presented by Emoricha *et al.* (2010).

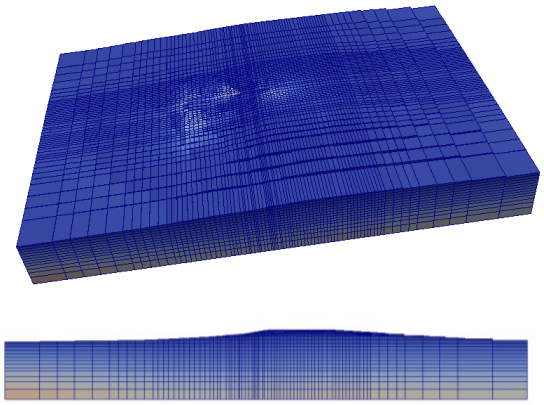

Figure 2: Computational grid for the Mt. Apo model

The permeability distribution for the initial model was based on the permeability values used in Mt. Apo simulation study of Emoricha *et al.* (2010). The permeability and porosity were later adjusted manually and by inverse modeling using PEST to improve the model. The linear relative permeability function was used with the following parameters: immobile liquid and vapor saturation values of 0.2 and 0.1 respectively; and perfectly mobile liquid and vapor saturation values of 0.9 and 0.7 respectively. The boundary conditions for the top of the model are a pressure of 0.1 MPa and a constant temperature of 65°C. The natural-state model was run to an end time of 1E14 seconds (3.169 million years) to attain steady-state conditions. The production history simulations were carried out with a constant time step of 2.628E6 seconds.

3.2.2 Dual porosity model

For the dual porosity model, the secondary mesh for the embedded matrix blocks was created with GMINC (Pruess, 2010). The partitioning of a block of the single porosity model was made in such a way that the first volume fraction corresponds to the fracture while the remainder of the volume was assigned to the matrix.

Two forms of grid partitioning were created for the dual porosity models to test the effect of varying the volume fraction occupied by the fracture:

(a) Model 1 has a fracture volume fraction of 2% while the rest of the volume was assigned to two matrix blocks with volume fractions of 20% and 78% respectively.

(b) Model 2 has a fracture volume fraction of 1% while the rest of the volume was assigned to two matrix blocks with volume fractions of 20% and 79% respectively.

The two-phase liquid-dominated zone and the high enthalpy and steam-dominated zone were formed in the layers where the feedzones of the production wells are located and single-phase conditions remain in other deeper layers throughout the history matching period. Thus the dual porosity method was applied only to 8 layers of the model where the feedzones of the production wells are located (layers 9, 10, 11, 12, 13, 14, 15, and 16).

As well as the 57,125 elements of the single porosity model, both dual porosity Models 1 and 2 have an additional 56,880 matrix elements (8 layers x 3,555 blocks x 2 nested matrix layers) for a total of 114,005 elements. It would be possible to modify the model further by reducing the number of blocks that are converted to dual porosity blocks, recognising that only a portion of connected fractures may be active in conducting water. For example, it is probably not necessary to use a dual porosity grid outside the hot reservoir.

3.3 Model parameters

The fracture was assigned a very high porosity fixed at 90%. The matrix porosity values were based on porosities used in the single porosity production history model. The initial matrix porosity was chosen such that effective porosity of the dual porosity model is the same as the porosity of the single porosity model (See Eqn. 1):

$$\theta_{eff} = \theta_f V_f + \theta_m (1-V_f) \qquad (1)$$

Where θ_{eff}, θ_f, and θ_m are the effective, fracture, and matrix porosities respectively and V_f is the fraction of the total block volume occupied by the fractures. The initial fracture permeabilities were given the same values as the final values of the single porosity production history model. The matrix permeabilities were assigned a value of 5 micro-Darcy (0.5E-17m^2). The initial parameters used with the dual porosity model are summarized in Table 1.

Table 1: Initial parameters used with the dual porosity model

Parameters		Model 1	Model 2
Volume fraction	Fracture	2%	1%
	Matrix 1	20%	20%
	Matrix 2	78%	79%
Permeability (m^2)	Fracture	Varies according to single porosity model values	
	Matrix	0.5E-17	0.5E-17
Porosity	Fracture	0.9	0.9
	Matrix	Varies according to single porosity model values, θ_{eff} (1)	
Rock grain density (kg/m^3)		2500	2500
Rock specific heat (J/kg K)		1000	1000
Rock conductivity (W/m K)		2.5	2.5
Relative permeability		[2]Linear: S_{lr} = 0.2, S_{vr} = 0.1, S_{lm} = 0.9, S_{vm} = 0.7	

Note: (1) immobile liquid saturation (S_{lr}), immobile vapor saturation (S_{vr}), perfectly mobile liquid saturation (S_{lm}), and perfectly mobile vapor saturation (S_{vm}).

4. MODEL CALIBRATION

4.1 Initial manual calibration

First some adjustment to the parameters was made to ensure that the single and dual porosity model runs reached the target end time. Then the natural-state model was calibrated manually by adjusting the permeability values until the model results approximately match the steady-state temperature and pressure data. Similarly, the production-history model was calibrated manually by adjusting the permeability and porosity values until the model results approximately matched the transient enthalpy data.

4.2 Automatic model calibration using PEST

When the results from the natural-state and production history simulation approximately matched the observed data, a switch was made to automated calibration using the computer program PEST (Doherty, 2010). PEST was used for parameter estimation in order to obtain the best fit of both the single and dual porosity models to the data and to allow a quantitative comparison of the results from the best single porosity and best dual porosity models.

Whereas in manual calibration model parameters are estimated by trial-and-error and the judgment of the modeller, PEST estimates the optimal parameter values by minimizing the objective function calculated as the sum of weighted, squared, differences between simulated model values and data from field measurements. PEST make use of truncated singular value decomposition (SVD)

supplemented, where necessary, with Tikhonov regularization (Doherty, 2010). The website *www.pesthomepage.org* allows access to the PEST manual which describes how to use PEST.

4.3 Parameters estimated by PEST and calibration data

Parameters to be estimated by PEST for the single porosity model

For the single porosity model, the parameters to be estimated were: *(a)* permeabilities in the x and z direction for 117 rock-types; and *(b)* porosities for 117 rock-types. The model is horizontally isotropic and hence the permeability in the x and y direction for the 117 rock-types are tied; thus there were 234 and 351 parameters for PEST to estimate for the natural state and production history models, respectively. The total number of observations is 2,234 consisting of 1,434 temperature and pressure data points and 800 production enthalpy data points.

Dual porosity model parameters to be estimated by PEST

For the dual porosity model, the parameters to be estimated were: *(a)* fracture and matrix permeabilities in the x and z direction for 117 rock-types; and *(b)* fracture and matrix porosities for 117 rock-types. Not all the rock-types were present in the blocks that were converted to dual porosity and thus there were only 936 parameters for PEST to estimate. The fracture permeabilities and porosities and matrix permeabilities and porosities were adjusted to match the transient production enthalpy data.

4.5 Challenges with model calibration using PEST

Using PEST to improve the calibration of the model of the Mt. Apo geothermal reservoir proved to be difficult for several reasons.

(i) *Model failure*. In some cases the forward model would not run until the target end time. Low permeabilities near the production wells are required to achieve a large enough pressure drop to induce boiling and a high production enthalpy but if the permeabilities are too low the pressure drops too low and the simulation does not finish.

(ii) *Numerical convergence problems can occur in blocks where phase transitions are taking place.* There are blocks where phase change takes place and the block switches between single-phase and two-phase at each Newton iteration causing AUTOUGH2 to reduce the time step drastically which increases the time required to complete a simulation run.

(iii) *The parameter estimation process is computationally demanding.* In the beginning for the dual porosity models, when parameters were far from their optimum values, it took a forward run of AUTOUGH2 almost six hours to finish because very small time steps were required. Whereas for the single porosity model, it took a forward run of AUTOUGH2 only one hour to finish. Moreover, the dual porosity model has ~3 times more parameters to estimate, which requires more forward runs per iteration of parameter adjustment.

(i) Scheme for rejecting model failures

For cases when the natural-state model has not reached the desired end time, the LISTING file is deleted and the natural state model is run again in order to ensure that the outputs for models runs that do not finish do not corrupt the calculation of the derivatives required for parameter updating.

In order to reject AUTOUGH2 runs that do not reach the set end time and to allow the optimization process to proceed when a model run failure is encountered, the "derforgive" and "lamforgive" variables were included in the PEST control file. The "derforgive" variable accommodates a total or partial model failure during a Jacobian calculation run by setting important parameter sensitivities to zero. With "derforgive", a "dummy" model output value is provided which does least harm to the derivative. On the other hand, the "lamforgive" variable treats a model run failure during testing of parameter upgrades in the lambda search as a high objective function. This provides PEST with a disincentive to use parameter values which are close to the parameter space which has been demonstrated to result in problematical model behavior. By rejecting unfinished model runs, these PEST settings ensured that the optimization runs were terminated because the objective function could no longer be improved and not because of a series of failed forward runs.

(ii) Feedzone pressure as a parameter for optimization

In order to resolve the problem of switching from single-phase to two-phase conditions, the difference between the block pressure and the saturation pressure at the feedzone was included as part of the objective function for PEST to minimize. The minimization of the difference between the block pressure and the saturation pressure at the feedzone effectively drives the block towards boiling. If the block is already boiling, then the difference between the block pressure and the saturation pressure is zero. In cases when the block is in superheated condition and the block has a negative pressure, the pressure in the block is reset and made equal to the saturation pressure which effectively makes the difference between the block pressure and the saturation pressure equal to zero.

(iii) Parallelization

The optimization of the parameters for the dual porosity production models is computationally demanding. At the start of the simulation for the case of the dual porosity production models when parameters were far from their optimum values, it took a forward AUTOUGH2 run almost 6 hours to finish because of the large number of computational blocks. There are 963 parameters to estimate which required 963 forward AUTOUGH2 runs in order to complete one optimization run. The total computation time is thus 5,778 hours or almost 241 days.

In order to speed up the parameter estimation process, parallelization of the AUTOUGH2 model runs was adopted by implementing a special version of parallel PEST called BEOPEST (Schreüder, 2009). BEOPEST creates an improvised cluster on the fly. In BEOPEST, the master process performs the parameter estimation, sends the parameters for the input files to be run to the subordinate cluster, and receives model results back from the subordinate in binary form via a transmission control protocol/

internet protocol (TCP/IP) connection. The subordinate creates AUTOUGH2 model input files from the parameters given by the master, runs the AUTOUGH2 forward model, extracts the results from the AUTOUGH2 model listing/output files, and sends the simulation results back to the master. As a result, much of the computational load is offloaded to the subordinate computers and only the parameter estimation proper is left to the master.

With a single processor that can complete four forward runs in a day, the estimated computational time is 60.2 days which is still too long to be acceptable. To shorten the computational time, BEOPEST was run remotely on EDC's parallel computing cluster which was later supplemented by the New Zealand e-Science Infrastructure or NeSI PAN cluster. The parallelization of the AUTOUGH2 model runs using BEOPEST and running on a 2x32-core parallel computing clusters effectively reduced the computational time to 9 days which included ~7 days for completing the forward runs plus another two days for processing the results and giving the results back to BEOPEST.

(iv) Super parameters

There are 351 adjustable parameters for PEST to estimate for the single porosity production history model. In comparison, there are 936 adjustable parameters for PEST to estimate for the dual porosity production history models because of the inclusion of the secondary mesh for the embedded matrix blocks. The objective function is minimized by PEST using the truncated singular value decomposition (SVD) supplemented, where necessary, with Tikhonov regularization. Truncated SVD simplifies the problem by estimating combinations of parameters (super-parameters) rather than the parameters themselves (Doherty, 2010). Truncated SVD gives higher priority to numerical stability compared to other factors when solving an inverse problem.

The calibration of Mt. Apo reservoir model used the SVD-assist utility of PEST which combines the strength of the two regularization methods. The calibration process uses super-parameters with SVD-assist which are linear combinations of the original parameters (permeability and porosity of the rocks). The use of SVD-assist decreased the number of parameters, and thus the number of forward model runs required to optimize the single porosity production model, from 351 to 135 and the number of forward model runs required to optimize the dual porosity production model from 936 to 200.

5. MODELS OF THE MT. APO RESERVOIR

The Mt. Apo geothermal reservoir was represented using a single porosity model and two dual porosity models. The models that were investigated are summarized in Table 2.

Table 2: Summary of dual porosity models of the Mt. Apo geothermal reservoir

Parameters		Model 1	Model 2
No. of elements		114,005	114,005
No. of matrix blocks		2	2
Volume fraction	Fracture	2%	1%
	Matrix 1	20%	20%
	Matrix 2	78%	79%
Permeability (m^2)	Fracture	Varies according to single porosity model values (final values are in Fig. 9)	
	Matrix	0.5E-17	0.5E-17
Porosity	Fracture	0.9	0.9
	Matrix	Varies according to single porosity model values, $^1por_{eff}$	
Parameters optimized		(a) Fracture and matrix permeability; (b) Fracture and matrix porosity	

6. SIMULATION RESULTS AND DISCUSSION

6.1 Natural-state single porosity model results

With the parameter estimation process using PEST, the objective function was reduced from an initial value of 43,511 to 33,431 for the best single porosity natural-state model. The simulated pressure and temperature results were compared against the steady-state pressure and temperature data for wells from different sectors of the reservoir such as the upflow zone, main productive field, buffer area, and the injection sink. The temperature and pressure profile matches were significantly improved for most of the wells. The matches of temperature and pressure for some of the wells from different areas in the reservoir are shown in Figure 3.

A vertical slice plot shows the temperature distribution from the Sandawa to Matingao sector and liquid mass flows from -3000 mrsl to water level (See Figure 4A.) The figure shows the hottest part of the resource (~330°C) is beneath the Sandawa collapse. The highest liquid mass flux is assigned beneath the caldera. The liquid mass flux vectors show that the water flows laterally and come out at the surface where the major outflow features such as the thermal springs in Agco, Imba and Marbel are located. From the plots of temperature distribution and direction of mass flux vectors, it is seen that the natural-state model is consistent with the conceptual model.

The natural-state model was able to replicate the formation of a natural steam zone within the shallow levels of the Sandawa collapse, ranging from ~250 mrsl upwards. The plots of the vapor saturation at different model layers are shown in Figure 4B.

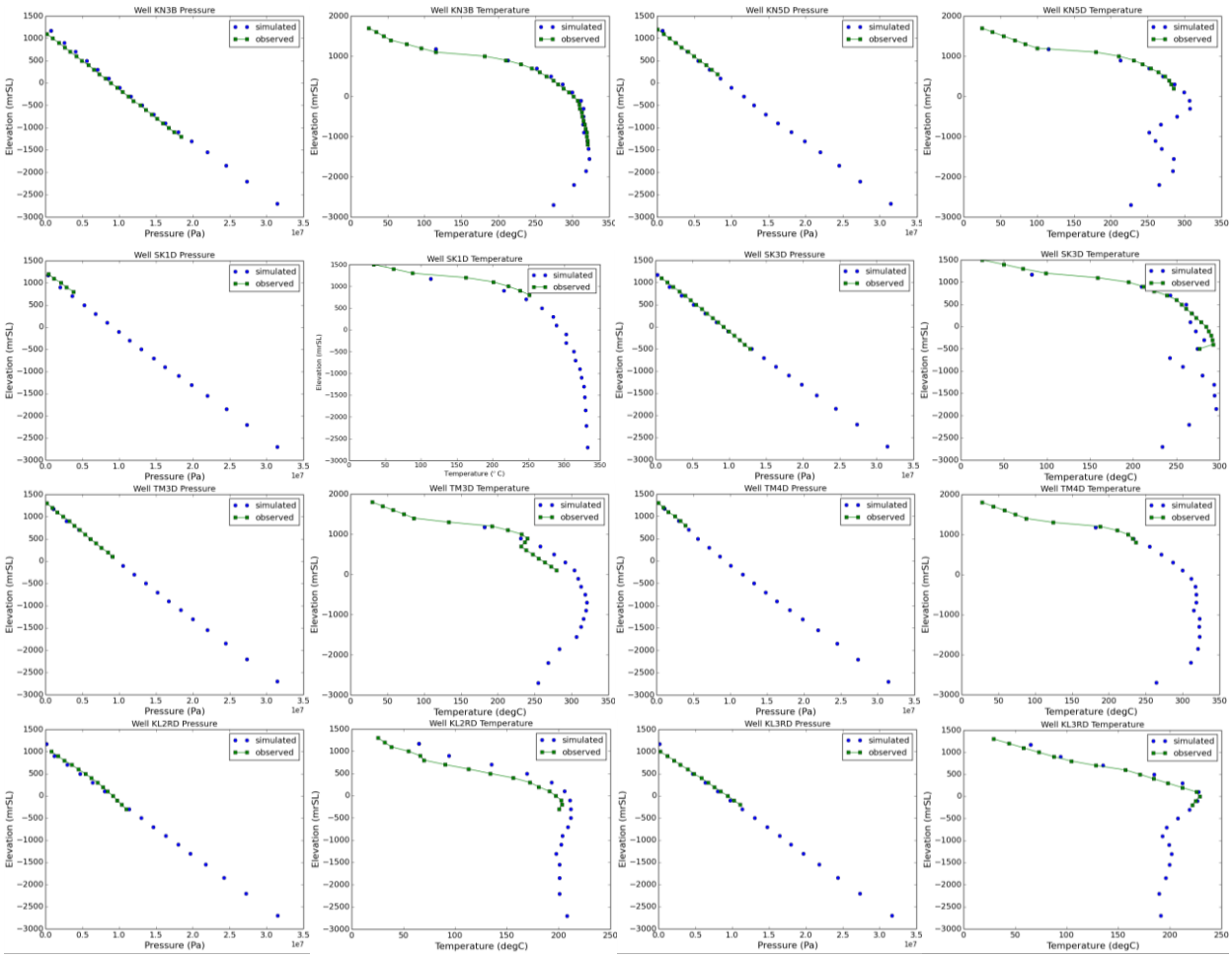

Figure 3: Match of temperature and pressure of the single porosity NS model for wells in: (*a, 1st row)* the upflow zone, (*b, 2nd row)* the main productive field (*c*, 3rd row*)* the buffer area, and (*d, 4th row)* the injection sink

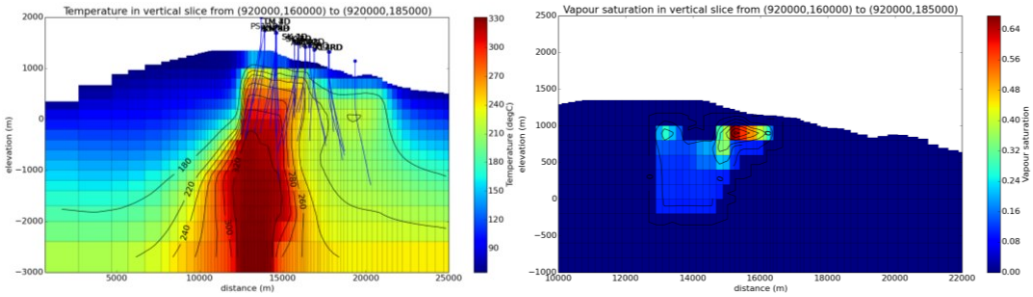

Figure 4: Vertical slice through the single porosity natural-state model showing: (A) the temperature distribution along the Sandawa to Matingao sector and the mass flow from -3000 mrsl to water level and (B) the formation of two-phase zones from layer 11 at -160 mrsl to layer 17 at 1000 mrsl.

6.2 Production history model results: single and dual porosity models

Both the best single porosity model and the best dual porosity model were able to match the enthalpy transients of wells with two-phase liquid-dominated discharge quite well as seen from the enthalpy plots for wells APO1D and SK2D (See Figure 5.) The wells were modeled with multiple feedzones (16 of them) while the rest were modeled with a single feed zone.

The single porosity model, however, was unable to provide a consistent match to the enthalpy transients of the two-phase steam-dominated wells because the modeled enthalpy drops at some point in time as a result of the entry of low-enthalpy recharge fluids. Furthermore, the single porosity model overestimated the enthalpy for well KN2D from year 6 to year 16.2 by as much as ~200kJ/kg. On the other hand, the model underestimated the enthalpy for well KN3B from year 2 to year 10 by as much as ~500kJ/kg. Nevertheless, the best single porosity model provided a reasonable model as a starting point for the dual porosity model.

The dual porosity model was able to reasonably fit all the production enthalpy data: *(1)* the measured enthalpy of wells with two-phase liquid-dominated discharge as shown in the plots for wells APO1D and SK2D; and *(2)* wells with two-phase steam-dominated discharge as shown in the plots for wells SK1D, KN2D, KN3D, KN5D, TM3D, and TM4D. In particular the dual porosity model was able to provide a better match to the enthalpy transients of the two-phase steam-dominated wells like SK1D, TM3D, and TM4D than was achieved with the single porosity model. Furthermore, the dual porosity model was also able to match the increase in enthalpy of well KN5D which was not achieved by the single porosity model.

The plots comparing the simulated enthalpy results with enthalpy data for the single porosity model and dual porosity models, with 2-matrix and fracture volume fraction of 2% and 2-matrix with fracture volume fraction of 1%, are shown in Figure 5.

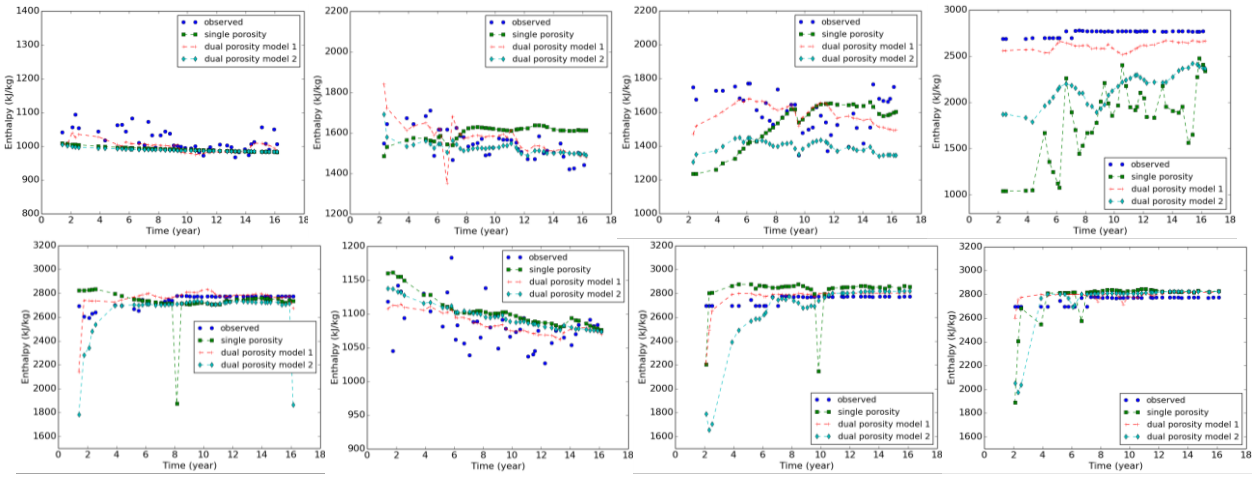

Figure 5: Match of the enthalpy transients for the single and dual porosity models calibrated by PEST for wells (from left to right, top) APO1D, KN2D, KN3B, KN5D and (from left to right, bottom) SK1D, SK2D, TM3D, and TM4D

Both the single porosity model and dual porosity models were able to match the declining enthalpy trends of some of the wells, resulting from the effects of the injected brine. This trend is seen in APO1D, APO3D, SK2D, and SP4D, as reported by (Esberto *et al.*, 2001; Nogara and Sambrano, 2005). However, the effect of the injected brine return on enthalpy was not properly captured by the model in some of the wells (e.g. APO2D, MD1D, SK6D, and SK7D). In order to properly represent the effect of the injected brine on the enthalpy trends of all affected wells the rock-types assigned to the relevant blocks should be refined.

Comparison of the objective function

The single porosity production model started with an objective function of 73,313 which was eventually lowered to 19,083 after PEST made changes to the permeabilities and porosities of the model. The optimization runs were terminated by PEST when the objective function could no longer be improved. The best single porosity model, i.e. the model with the lowest value of the objective function, was converted to a dual porosity model and the fracture and matrix permeabilities and porosities were given to PEST to estimate.

Model 1 which has a fracture volume fraction of 2% gave an objective function of 11,105 after six optimization steps which is an improvement of 42% compared to the objective function given by the single porosity model. Model 2 which has a fracture volume fraction of 1% gave an objective function of 13,964 after five optimization steps which is 27% lower than the objective function given by the single porosity model. As shown in Figure 6 the objective function for Model 2 dropped more quickly than the objective function for Model 1 but seems to be leveling off at a higher value.

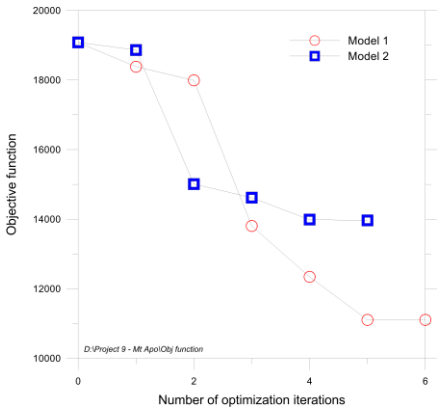

Figure 6: Improvement in the objective function per optimization iteration

Additional optimization runs were no longer pursued when the improvement in the objective function started to plateau after several optimization steps. A comparison of the values of the objective function for each model is shown in Table 4.

The temperature distribution from the Sandawa to Matingao sector after 16.2 years of production does not vary much for both single and dual porosity models as shown by the vertical slice plot in Figure 7 (A and B). The temperature inversion as a result of injection in the Matingao and Kullay sectors as described by Emoricha *et al.* (2010) can be seen on this plot.

The extent of the two-phase region was expanded and the vapor saturation of the two-phase region increased during the production of the field compared to when the reservoir was undisturbed (See Figure 4B). The expansion of the two-phase zone can be seen on

both single and dual porosity models (See Figure 8 A and B.) Higher vapor saturation (>90%) was obtained with the dual porosity model compared to the single porosity models from blocks that are representing wells with two-phase steam-dominated discharge.

Table 4. Comparison of objective function after parameter optimization using PEST

Model, type/parameters	[a] Single porosity	Dual porosity	
		Model 1	Model 2
Obj. f(x)	19,083	11,105	13,964
Number of optimization steps	15	6	5

Note: [a] The objective function of the single porosity production model before PEST optimization is 76,058

The histograms of the permeability values from the best single porosity and the fracture permeabilities from the best dual porosity model (Model 1) are shown in Figure 9B. Compared to the permeability distribution of the best single porosity model (see Figure 9A), the permeability distribution of the best dual porosity model have ~10% more of very low permeability rocks (1E-16), ~10% more of low permeability rocks (1E-15), ~20% less of medium permeability rocks (1E-14), and about 1% more of high permeability rocks (k > 1E-12).

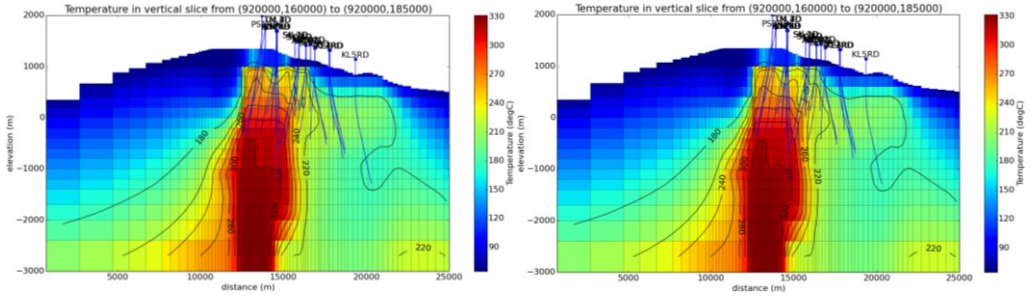

Figure 7: Vertical slices of (A) the best single porosity (left) and (B) the best dual porosity (right) production models showing the temperature distribution along the Sandawa to Matingao sector

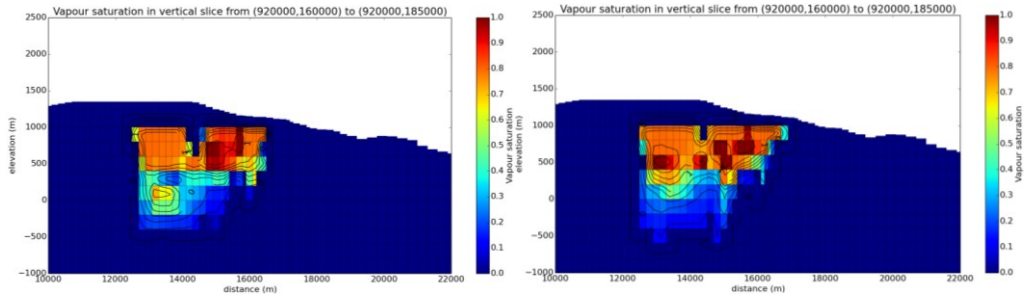

Figure 8: Vertical slices of (A) the best single porosity (left) and (B) the best dual porosity (right) production models calibrated by PEST showing the expansion and increase in vapor saturation of the two-phase zones

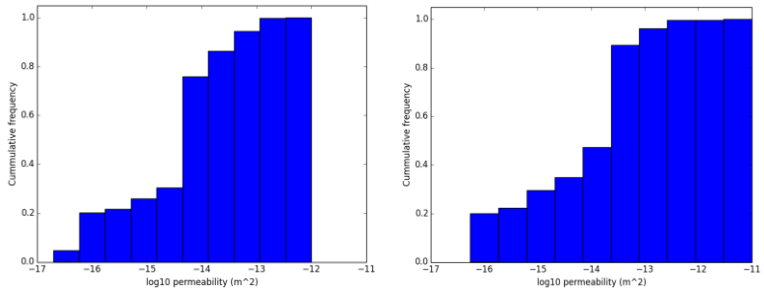

Figure 9: Histogram of (A) the x (=y) permeability values for the best single porosity (left) and (B) the fracture permeability of all the dual porosity blocks from the best dual porosity (right) model calibrated by PEST

7. CONCLUSIONS AND RECOMMENDATIONS

Both the best single porosity model and the best dual porosity model were able to match the enthalpy transients of wells with two-phase liquid-dominated discharge reasonably. However, the single porosity model was not able to provide a consistent match to the enthalpy of the two-phase steam-dominated wells.

The best dual porosity model proved to be the preferred model for modeling the two-phase geothermal reservoir of Mt. Apo because it clearly fitted the data better. The best dual porosity model was able to reasonably fit the flowing enthalpy data of wells with two-phase liquid-dominated discharge and it was able to produce very high vapor saturations (> 90%) in the blocks containing the feedzones of the two-phase steam-dominated wells and thus was able to match the production enthalpy data for wells with two-phase steam-dominated discharge. In particular the best dual porosity model was able to provide a more consistent match to the enthalpy transients of the two-phase steam-dominated wells like SK1D, TM3D, and TM4D compared to the single porosity model.

The best dual porosity model was also able to match the increase in enthalpy of well KN5D which was not achieved by the single porosity model.

And lastly, the best dual porosity model was able to reduce the objective function to a lower value than was achieved with the single porosity model. Model 1, which has a fracture volume fraction of 2%, yielded an objective function of 11,105 which is an improvement of 42% compared to the objective function of 19,083 for the single porosity model.

ACKNOWLEDGEMENTS

This research was carried out at the University of Auckland. The first author would like to thank the Energy Development Corporation for supporting this Doctoral study and for allowing him to use the Mt. Apo field data and publish this paper. The first author would also like to thank the University of Auckland for allowing him to use the NeSI PAN Cluster.

REFERENCES

Austria, J.J.C., 2008. Production Capacity Assessment of the Bacon-Manito Geothermal Reservoir, Philippines. United Nations University, Geothermal Training Programme.

Barenblatt, G.I., Zheltov, I.P. and Kochina, I.N., 1960. Basic concepts in the theory of seepage of homogeneous liquids in fissured rocks. Journal of Applied Mathematical Mechanics, 24(5): 1286-1303.

Bjornsson, G., Hjartarson, A., Bodvarsson, G.S. and Steingrimsson, B., 2003. Development of a 3-D geothermal reservoir model for the greater Hengill volcano in SW-Iceland. Citeseer.

Bodvarsson, G.S., Pruess, K., Stefansson, V., Bjornsson, S. and Ojiambo, S.B., 1987. East Olkaria geothermal field, Kenya. 1. History match with production and pressure decline data. Journal of Geophysical Research, 92(B1): 521-539.

Bodvarsson, G.S. and Witherspoon, P.A., 1985. Flow rate decline of steam wells in fractured geothermal reservoirs, Lawrence Berkeley Lab., CA (USA).

Bowyer, D. and Holt, R., 2010. Case Study: Development of a Numerical Model by a Multi-Disciplinary Approach, Rotokawa Geothermal Field, New Zealand, World Geothermal Congress 2010, Bali, Indonesia.

Buning, B.C., Malate, R.C.M., Austria, J.J.C., Noriega, M.T. and Sarmiento, Z.F., 1997. Casing perforation and acid treatment of well SK-2D Mindanao 1 Geothermal project, Philippines, Proceedings of the 22nd Workshop on Geothermal Reservoir Engineering, Stanford University, Stanford, CA, USA, pp. 273-277.

Butler, S.J., Sanyal, S.K., Henneberger, R.C., Klein, C.W., Puente, H. and de Leon, J., 2000. Numerical Modeling of the Cerro Prieto Geothermal Field, Mexico. Transactions - Geothermal Resources Council: 401-406.

Clearwater, J., Burnell, J. and Azwar, L., 2012. Modelling of the Ngatamariki Geothermal System, Thirty-Seventh Workshop on Geothermal Reservoir Engineering, Stanford University, Stanford, California.

Doherty, J., 2010. PEST: Model-Independent Parameter Estimation. Watermark Numerical Computing, Brisbane.

Emoricha, E.B., Omagbon, J.B. and Malate, R.C.M., 2010. Three Dimensional Numerical Modeling of Mindanao Geothermal Production Field, Philippines, Stanford Thirty-Fifth Workshop on Geothermal Reservoir Engineering, Stanford University, Stanford, California.

Esberto, M.B., 1995. Numerical simulation of the Mindanao 1 geothermal reservoir, Philippines. Diploma Thesis, University of Auckland, Auckland, 43 pp.

Esberto, M.B., Nogara, J.B., Daza, M.V. and Sarmiento, Z.F., 1998. Initial response to exploitation of the Mt. Apo geothermal reservoir, Cotabato, Philippines, Twenty-third Work shop on Geothermal Reservoir Engineering. SGP-TR-158, Stanford University, Stanford, California.

Esberto, M.B. and Sarmiento, Z.F., 1999. Numerical modelling of the Mt. Apo Geothermal Reservoir, Twenty-Fourth Workshop on Geothermal Reservoir Engineering, Stanford University.

Finsterle, S., Björnsson, G., Pruess, K. and Battistelli, A., 1999. Evaluation of geothermal well behavior using inverse modeling. Dynamics of Fluids in Fractured Rock, Geophysical Monograph, 122: 377-387.

Jaimes-Maldonado, J.G., Velasco, R.A.S., Pham, M. and Henneberger, R., 2005. Update report and expansion strategy for Los Azufres Geothermal Field, World Geothermal Congress, Antalya, Turkey.

Kiryukhin, A.V. and Miroshnik, O., 2012. Inverse modeling of the exploitation of the Mutnovsky Geothermal Field 1984-2006, Thirty-Seventh Workshop on Geothermal Reservoir Engineering, Stanford University, Stanford, California, January 30 - February 1, 2012.

Los Baños, C.F., Rigor, D.M.J., Layugan, D.B. and Bayrante, L.F., 2010. The Resistivity Model of the Mindanao Geothermal Project, South Central Mindanao, Philippines, World Geothermal Congress, Bali, Indonesia.

Molina, P.O., Malate, R.C.M., Buning, B.C., Yglopaz, D.M., Austria, J.J.C. and Lacanilao, A.M., 1998. Productivity analysis and optimization of well SK-2D, Mindanao I geothermal project Philippines, Proceedings of the 23rd Workshop on Geothermal Reservoir Engineering, Stanford University, Stanford, CA, USA, pp. 368-374.

Monterrosa, M.E. and SA, G.S., 2002. Reservoir Modelling for the Berlin Geothermal Field, El Salvador.

Nakanishi, S., Kawano, Y., Tokada, N., Akasaka, C., Yoshida, M. and Iwai, N., 1995. A reservoir simulation of the Oguni field, Japan, using MINC type fracture model, World Geothermal Congress pp. 1721-1726.

Nakao, S., Ishido, T. and Takahashi, H., 2007. Numerical simulation of tracer testing at the Uenotai Geothermal Field, Japan, Thirty-Second Workshop on Geothermal Reservoir Engineering, Stanford University, Stanford, California.

Narasimhan, T.N., 1982. Multidimensional numerical simulation of fluid flow in fractured porous media. Water Resources Research, 18(4): 1235-1247.

Nogara, J.B. and Sambrano, B.M.G., 2005. Tracer tests using naphthalene di-sulfonates in Mindanao geothermal production field, Philippines, World Geothermal Congress, Antalya, Turkey.

O'Sullivan, M.J., Yeh, A. and Mannington, W.I., 2009. A history of numerical modelling of the Wairakei geothermal field. Geothermics, 38(1): 155-168.

Ofwona, C.O., 2002. A Reservoir study of Olkaria East Geothemal System, Kenya United Nations University Geothermal Training Programme, Reykjavík, Iceland.

Okada, H. and Yamada, Y., 2002. Fracture distribution in and around intrusive rocks in the Fushime Geothermal Field, Japan: Evidence from FMI Logging, Society of Petrophysicists and Well-Log Analysts Annual Logging Symposium, 2002.

Osada, K., Hanano, M., Sato, K., Kajiwara, T., Arai, F., Watanabe, M., Sasaki, S., Sako, O., Matsumoto, Y. and Yamazaki, S., 2010. Numerical Simulation Study of the Mori Geothermal Field, Japan.

Pham, M., Klein, C., Ponte, C., Cabeças, R., Martins, R. and Rangel, G., 2010. Production/Injection Optimization Using Numerical Modeling at Ribeira Grande, São Miguel, Azores, Portugal, World Geothermal Congress 2010, Bali, Indonesia.

Porras, E.A., Tanaka, T., Fujii, H. and Itoi, R., 2007. Numerical modeling of the Momotombo geothermal system, Nicaragua. Geothermics, 36(4): 304-329.

Pritchett, J.W., 2005. Dry-steam wellhead discharges from liquid-dominated geothermal reservoirs: A result of coupled nonequilibrium multiphase fluid and heat flow through fractured rock. Geophysical monograph, 162: 175-181.

Pruess, K., 1983. Development of the general purpose simulator MULKOM. Earth Sciences Division Annual Report 1982, Lawrence Berkeley Laboratory Report LBL-15500.

Pruess, K., 1991. TOUGH2: A general-purpose numerical simulator for multiphase nonisothermal flows, Lawrence Berkeley Lab., CA (United States).

Pruess, K., 2010. GMINC - A Mesh Generator for Flow Simulations in Fractured Reservoirs. Lawrence Berkeley National Laboratory, LBNL Paper LBL-15227.

Pruess, K. and Narasimhan, T.N., 1985. A Practical Method for Modeling Fluid and Heat Flow in Fractured Porous Media Society of Petroleum Engineers, Volume 25, Number 1.

Sarmiento, Z.F. and Björnsson, G., 2007. Reliability of early modeling studies for high-temperature reservoirs in Iceland and the Philippines, Proceedings: Thirty Second Workshop on Geothermal Reservoir Engineering, Stanford University, Stanford, California. January, pp. 2007.

Schreüder, W., 2009. Running BeoPEST, Principia Mathematica. Document can be found via the following website address: http://www. prinmath. com.

Steingrimsson, B., Bodvarsson, G.S., Gunnlaugsson, E., Gislason, G. and Sigurdsson, O., 2000. Modeling studies of the Nesjavellir geothermal field, Iceland, pp. 2899-2904.

Suryadarma, Dwikorianto, T., Zuhro, A.A. and Yani, A., 2010. Sustainable development of the Kamojang geothermal field. Geothermics, 39(4): 391-399.

Sussman, D., Javellana, S.P. and Benavidez, P.J., 1993. Geothermal energy development in the Philippines: An overview. Geothermics, 22(5-6): 353-367.

Trazona, R.G., Sembrano, B.G. and Esberto, M.B., 2002. Reservoir management in Mindanao geothermal production field, Philippines, Proceedings, 27th Workshop on Geothermal Reservoir Engineering. Stanford University, California, pp. 28-30.

Vinsome, P.K.W. and Shook, G.M., 1993. Multi-purpose simulation. Journal of Petroleum Science and Engineering, 9(1): 29-38.

Warren, J.E. and Root, P.J., 1963. The behavior of naturally fractured reservoirs. Old SPE Journal, 3(3): 245-255.

Williamson, K.H., 1990. Reservoir simulation of The Geysers geothermal field, Fifteenth Workshop on Geothermal Reservoir Engineering, Stanford University, Stanford, California, pp. 113-123.

Yani, A., 2006. Numerical Modelling of Lahendong Geothermal System, Indonesia, The United Nations University, Geothermal Training Programme, Reykjavík, Iceland.

Yeh, A., Croucher, A.E. and O'Sullivan, M.J., 2012. Recent Developments in the AUTOUGH2 Simulator, Proceedings TOUGH2 Symposium 2012, Berkeley, California.

Zimmerman, R.W., Hadgu, T. and Bodvarsson, G.S., 1996. A new lumped-parameter model for flow in unsaturated dual-porosity media. Advances in Water Resources, 19(5): 317-327.